NIST Technical Note
NIST TN 2285

Comparison of Flow Measurement Devices for Large Fire Experiments

Giovanni Di Cristina
Rodney A. Bryant

This publication is available free of charge from:
https://doi.org/10.6028/NIST.TN.2285

NIST NATIONAL INSTITUTE OF STANDARDS AND TECHNOLOGY
U.S. DEPARTMENT OF COMMERCE

NIST Technical Note
NIST TN 2285

Comparison of Flow Measurement Devices for Large Fire Experiments

Giovanni Di Cristina
Rodney A. Bryant
Fire Research Division
Engineering Laboratory

This publication is available free of charge from:
https://doi.org/10.6028/NIST.TN.2285

April 2024

U.S. Department of Commerce
Gina M. Raimondo, Secretary

National Institute of Standards and Technology
Laurie E. Locascio, NIST Director and Under Secretary of Commerce for Standards and Technology

NIST TN 2285
April 2024

Publication History
Approved by the NIST Editorial Review Board on 2024-03-05

How to Cite this NIST Technical Series Publication
Di Cristina Torres G, Bryant RA (2024) Comparison of Flow Measurement Devices for Large Fire Experiments. (National Institute of Standards and Technology, Gaithersburg, MD), NIST Technical Note (TN) NIST TN 2285. https://doi.org/10.6028/NIST.TN.2285

Author ORCID iDs
Giovanni Di Cristina Torres: 0000-0002-0799-3418
Rodney A. Bryant: 0000-0002-5344-9878

Abstract

Bi-directional probes are utilized throughout fire research and testing to measure fire-induced flows due to their ability to measure flow which changes direction, and to withstand hostile environments. However, they are not available commercially and researchers must acquire them through custom fabrication. S-type probes (S-probes) work on the same principle as bi-directional probes thereby offering the same benefits. However, S-probes also feature reliable manufacturing and calibration standards. For the first time the performance of bi-directional and S-probes are compared in side-by-side experiments. Measurements of a steady flow in a well-characterized wind tunnel were examined and the probes were used to measure the velocity profile across a turbulent jet from a blower fan. In both scenarios, the S-probe performed comparable to or better than the bi-directional probe in terms of accuracy. The results demonstrate the S-probe as a suitable alternative to the bi-directional probe for measurements of fire-induced flow.

Keywords

Fire-Induced Flow; Flow Calibration; Flow Speed Measurement; Pitot Probe

Table of Contents

List of Tables

Table 1: Test matrix. The flow speeds used in the wind tunnel (WT) and the spacing increments used along the wind jet (WJ) tests are denoted. **4**

Table 2: Uncertainty budget from the wind tunnel experiments at 4m/s showing the results from the three probes tested. The relative standard uncertainty is shown. **21**

Table 3: Uncertainty budget from the wind jet experiments at y = 15cm showing the results from the three probes tested. The relative standard uncertainty is shown. **22**

List of Figures

Acknowledgments

The authors gratefully acknowledge fabrication support provided by Marco Fernandez, engineering technician, and data acquisition support provided by Artur Chernovsky, electronics engineer.

1. Introduction

Fire research experiments create harsh and challenging conditions for diagnostic instrumentation. The instruments must be robust enough to withstand the smoke and high temperatures, while delivering accurate results. Robust probes such as thermocouples, heat flux gauges, and bi-directional probes, are commonly used to provide valuable measurements of temperature, heat flux, and flow, respectively. Flow measurements are necessary to quantify the transport of heat and smoke generated by a fire, and bi-directional probes are ubiquitous when measuring fire-induced flows [1–4]. The bi-directional probe is similar to the standard pitot probe as it is a differential pressure device used to infer flow velocity. The bi-directional probe was designed for the dirty and hostile fire environment, with the primary objective of conducting measurements in areas where the directionality of the flow is expected to shift, as the name implies. Large pressure openings (see Fig. 1) safeguard the probe from clogging by particulates and condensation, making it ideal for measurements in smoke laden flows. The large openings also make the probe less sensitive to flow angle, allowing it to be used without precise knowledge of flow orientation. Previous characterizations of the probe estimate its accuracy at 10 % when compared to a pitot-static probe [5, 6]. Despite the bi-directional probe being a very practical device for fire experiments, commercial development did not materialize. This resulted in researchers having to manufacture their own probes and rely on a limited set of characterizations from the literature [5, 6]. Hence an instrument important to the progress of fire research has existed without reliable manufacturing or calibration standards.

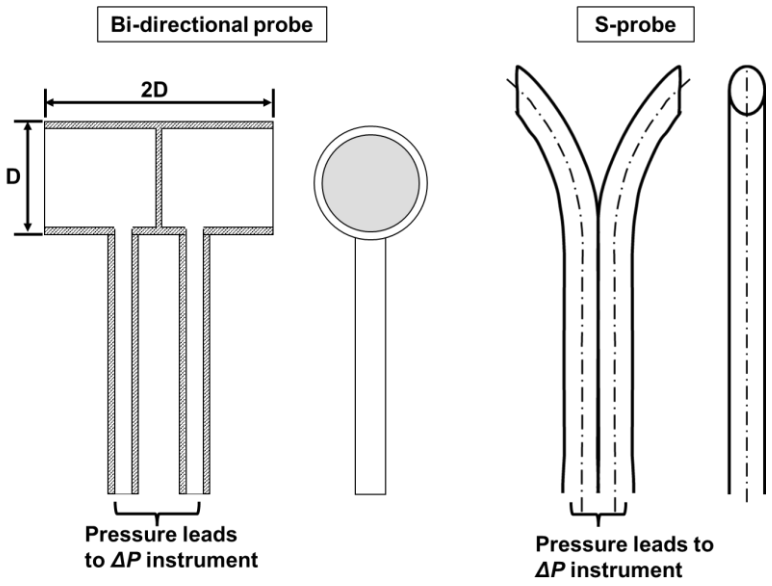

Fig. 1: Diagrams of a bi-directional probe (left) and S-probe (right).

Like the bi-directional probe, the S-probe was also designed for particle laden flows in harsh environments. It is comprised of two tubes of the same size with a cut-off bend, and each tube welded together. The upstream opening is subject to the total pressure and the downstream opening experiences a reduced pressure. This design provides the same benefits as the bi-

directional probes but with simpler construction and better accuracy. Frequent use of the S-probe did take hold in the emissions monitoring industry, and it became readily available from a variety of commercial sources. S-probes are manufactured with a range of diameters, lengths, and end connectors, providing researchers and practitioners with an off-the-shelf flow monitoring device for harsh environments. It is the primary device for providing reference flow measurements when auditing continuous emissions monitoring systems (CEMS) at the smokestacks of electric power plants [7]. The U. S. Environmental Protection Agency (EPA) has established dimensional requirements to standardize its production and therefore normalize its use across the emissions industry. The baseline calibration coefficient for S-probes manufactured according to these dimensional requirements is 0.84 [7], as determined from early investigations by the EPA and American Society for Testing and Materials (ASTM) for a host of S-probes with various geometries and physical conditions [8, 9]. The baseline coefficient has also been adopted by the International Organization for Standardization (ISO) [10].

Recent investigations have revisited the performance of the S-probe with respect to manufacturing quality and sensitivity to flow direction. This new interest in the S-Probe is due to global efforts to establish accurate emissions inventories and mitigate the impact of greenhouse gas emissions on climate change. Recent studies, when combined, have tested more than one hundred S-probes to determine the impact of geometry, manufacturing source, Reynolds number, and flow alignment on the calibration coefficient [11–13]. In all cases the calibration coefficient was within ±3 % of the baseline coefficient as long as the alignment of the probe axis and the bulk flow was within ±10°, misalignment beyond 10° increases the error above 5 % and increases with the angular deviation. Simulations of calibration experiments using computational fluid dynamics (CFD) demonstrated less than 2 % discrepancy between calibration coefficients determined from simulations and experiments, further supporting the accuracy of the baseline coefficient [14]. Studies such as these provide a large body of evidence to support the performance of the S-probe. Due to the well characterized performance and commercial availability, researchers have begun to utilize the S-probe to characterize fire induced flows. It has been utilized in recent investigations of fire whirls to measure air entrainment rates [15–17].

The characterization in this report is carried out in two steps. First, a well characterized wind tunnel is utilized to compare flow measurements from bi-directional and S-probes. The three probes are subject to 5 flow speeds (1, 2, 4, 6, 8 m/s)spanning the range typical of fire induced flows [2–4, 6]. For a subset of these speeds multiple S-probes are tested to examine variability due to previous use and geometry. Second, the three probes are subject to flow from a centrifugal blower - also known as a squirrel-cage fan. The fan provides flow turbulence and intermittency similar to realistic flow scenarios in fire environments. In both cases, the pitot-static probe serves as the reference flow measurement.

2. Materials and Procedures

Photos of the pitot probe, bi-directional probe, and S-probe are shown in Fig. 2. The pitot probes utilized have a 3.175 mm outer diameter with a 1 mm diameter total pressure port at

the tip. The static pressure ports are located 15 mm behind the total pressure port and the insertion length of the pitot probes is 30.5 cm.

The bi-directional probes were constructed from a 16 mm diameter tube cut to a length of 32 mm such that the openings have a diameter of 16 mm. A characteristic of bi-directional probes is that the aspect ratio (length to width) should remain at 2. A metal plate separates the total pressure and static pressure sides, and 4.76 mm outer diameter tubes are welded at the base of the probe which captures the respective pressure.

The S-probes tested here are composed of two 0.95 cm diameter tubes with a 45° bend that is cut-off making a perpendicular face with respect to the incoming flow. The tubes are welded along their respective spines, with each tube collecting either the total pressure or static pressure.

Each probe's total pressure and static pressure ports were then connected to the positive and negative sides, respectively, of a pressure transducer.

The flow velocity measurements from S-probes and bi-directional probes were compared against pitot probe results under two separate test conditions. The first, a wind tunnel (*WT*) with a well-conditioned, steady, uniform flow field. The second, an open wind jet (*WJ*) provided by a fan blower mounted on a table at a fixed distance from the probe under study. At each test condition, the manufacturing consistency was also examined by subjecting multiple probes (identified as A-E) of the same type. The test matrix is summarized in Table 1. The wind tunnel results show the idealized performance of each probe. While the wind jet tests show how the probes would respond in a more realistic environment. Additionally, two fouled S-probes and bi-directional probes were tested in order to determine how much of the use of the probes in a sooty or contaminated environment impact the probe response. The S-probes were fouled during velocity measurements of the NFRL exhaust system [18], while the bi-directional probes were fouled measuring the vent flow out of a large compartment fire [19].

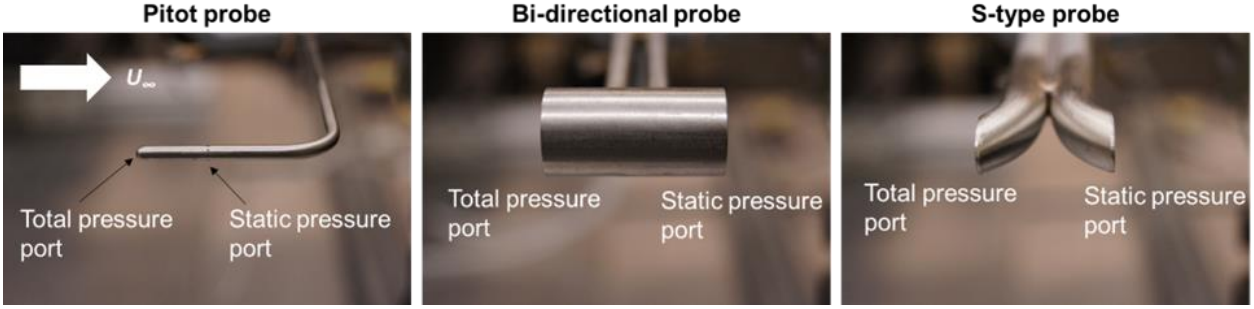

Fig. 2: The three velocity probes tested.

Table 1: Test matrix. The flow speeds used in the wind tunnel (WT) and the spacing increments used along the wind jet (WJ) tests are denoted.

Probe	A	B	C	D	E
Pitot	WT 1,2,4,6,8 m/s WJ 1cm	WT 1,2,4,6,8 m/s WJ 2cm	×	×	×
S-probe	WT 1,2,4,6,8 m/s WJ 1cm	WT 1,2,4,6,8 m/s WJ 2cm	WT 2,4,6 m/s ×	WT 2,4,6 m/s ×	WT 2,4,6 m/s ×
Bi-dir.	WT 1,2,4,6,8 m/s WJ 1cm	WT 1,2,4,6,8 m/s WJ 2cm	WT 2,4,6 m/s ×	WT 2,4,6 m/s ×	WT 2,4,6 m/s ×

2.1. Wind Tunnel

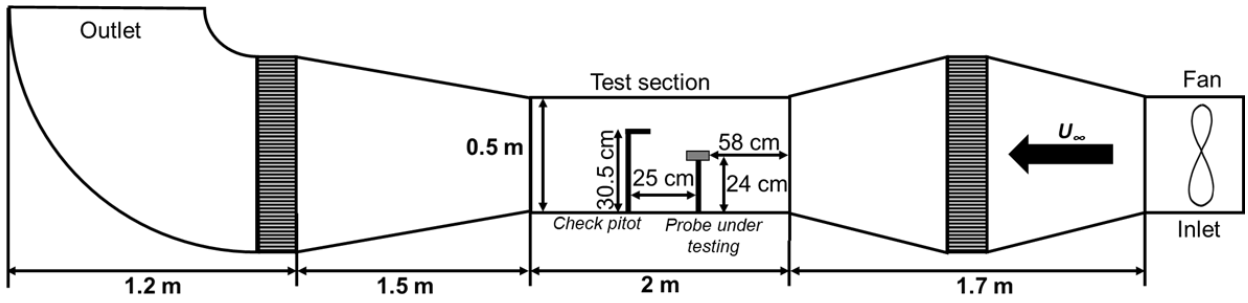

Fig. 3: Wind Tunnel schematic and probe configuration within the test section.

Wind tunnel testing was conducted at 1 m/s, 2 m/s, 4 m/s, 6 m/s, and 8 m/s to compare the S-probe and bi-dir. probe response to the pitot-static probe. A schematic of the wind tunnel used is shown in Fig. 3. The overall design is composed of the fan, a diverging - converging flow conditioning section, test section, and diverging section that exhausts into the room. The fan is powered by a 1.1 kW (1.5 HP) motor (Baldor EM3667T) controlled by a variable frequency driver (VFD) (Baldor VS1MD). The test section has a cross-sectional area of 0.5 m x 0.5 m and a total length of 2 m.

Probes under testing were installed 58 cm from the inlet to the test section, centered with respect to the width, and the center of each respective probe sensing area 24 cm above the bottom of the test section. A pitot probe was simultaneously collecting velocity data during wind tunnel tests. The check velocity pitot probe was installed 25 cm behind of the probe under testing, laterally offset by 6 cm, and 30.5 cm above the bottom of the test section.

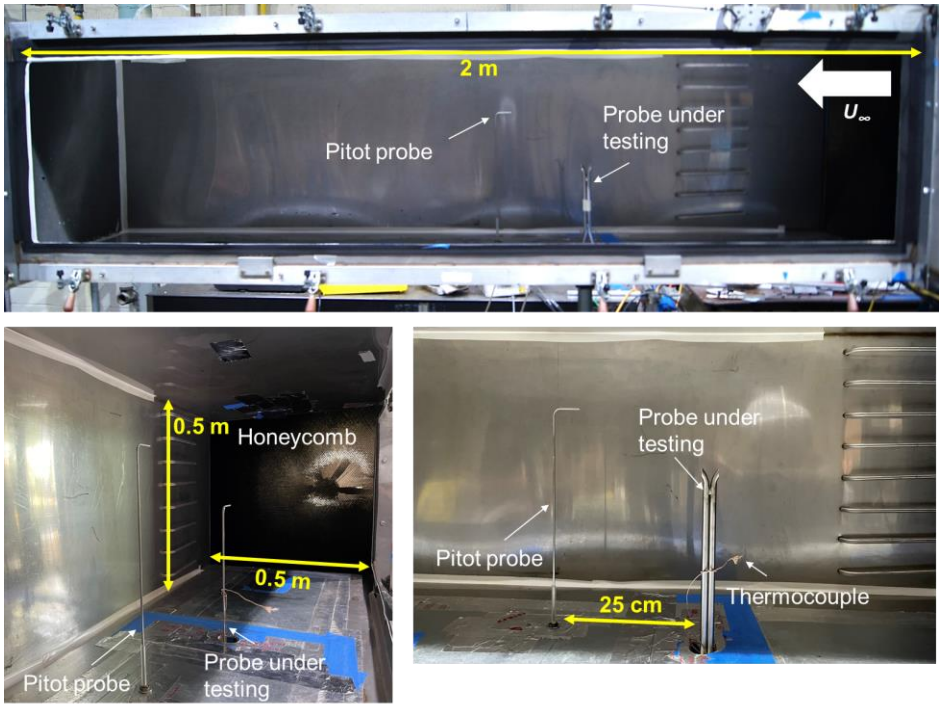

Fig. 4: Test section photographs showing various probes under testing and related dimensions.

The velocity range chosen corresponds to typical flow speeds encountered in fire-induced flows. Five different S-probes and bi-dir. probes were utilized for a subset of the flow speeds (2 m/s, 4 m/s, 6 m/s) to examine the impact of previous use and manufacturing variability. At each flow set point, data was collected for 300 s at 1 kHz and repeated three times. The set points for the wind tunnel tests are shown in Table 1 as *WT*.

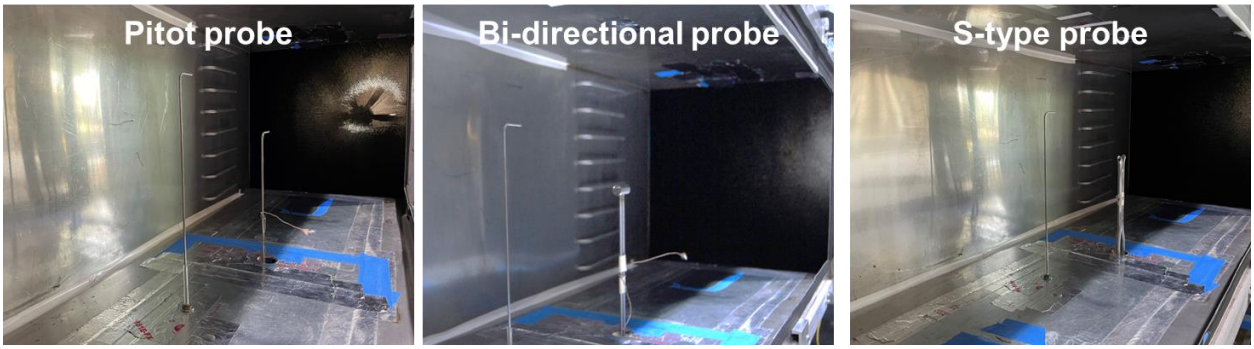

Fig. 5: The three kinds of probes tested, shown in the wind tunnel test section.

2.2. Wind Jet

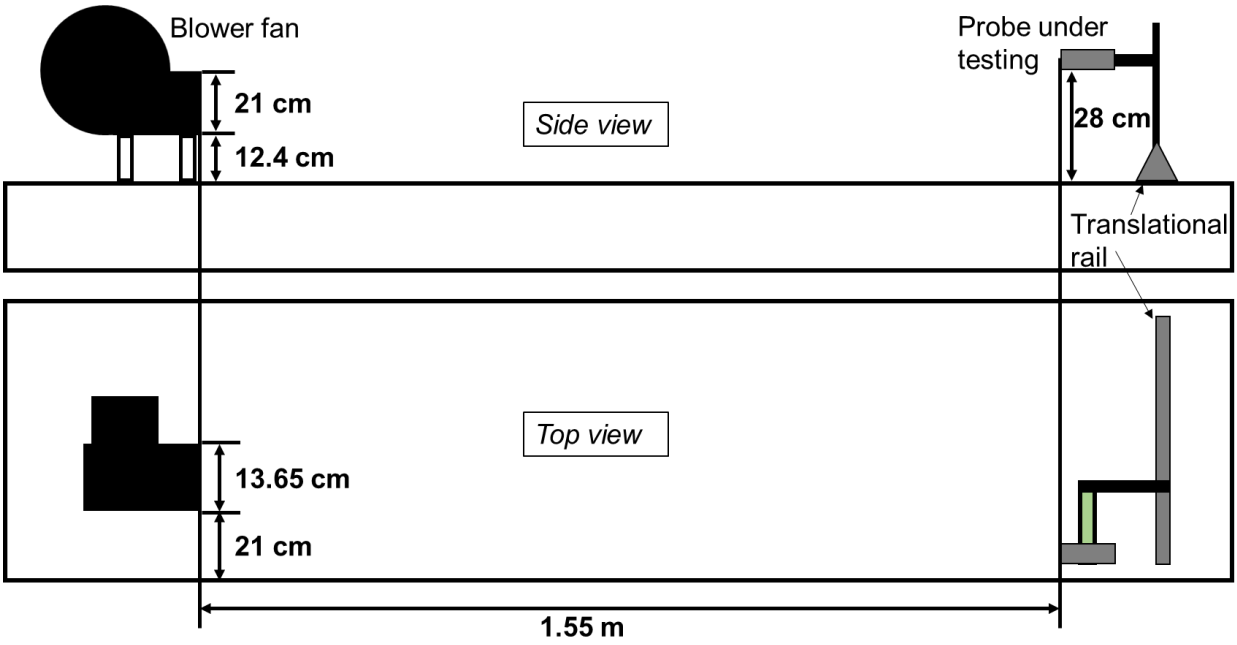

Fig. 6: Side and Top view of the Jet table setup.

For the wind jet tests, a blower fan powered by a 0.25 kW (1/3 HP) motor (Dayton 6K030G) was mounted to a table as shown in Fig. 6. The blower outlet has dimensions of 13.7 cm by 21.0 cm and was situated 12.4 cm above the table surface.

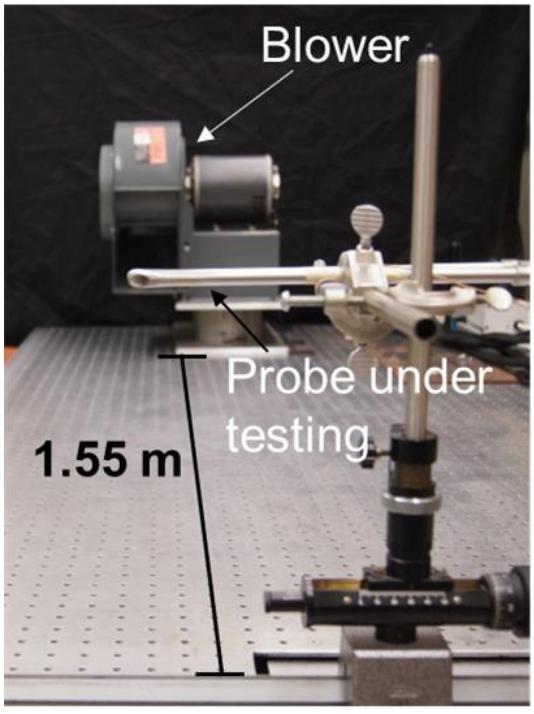

Fig. 7: Photograph positioned behind an S-probe under testing, showing the testing configuration with the blower and translational rail.

The probes were mounted 1.55 m away from the fan exit on a translational slide that moved perpendicular to the flow. The center of each probe's respective sensing area was 28 cm above the surface of the table. Two probes of each type were tested (A & B). Flow velocity was measured across a 47 cm span to map out the jet velocity at a high and low flow speed. The 'A' probes were moved at 1 cm increments and the 'B' probes at 2 cm increments, these are denoted in the test matrix (Table 1) as *WJ*.

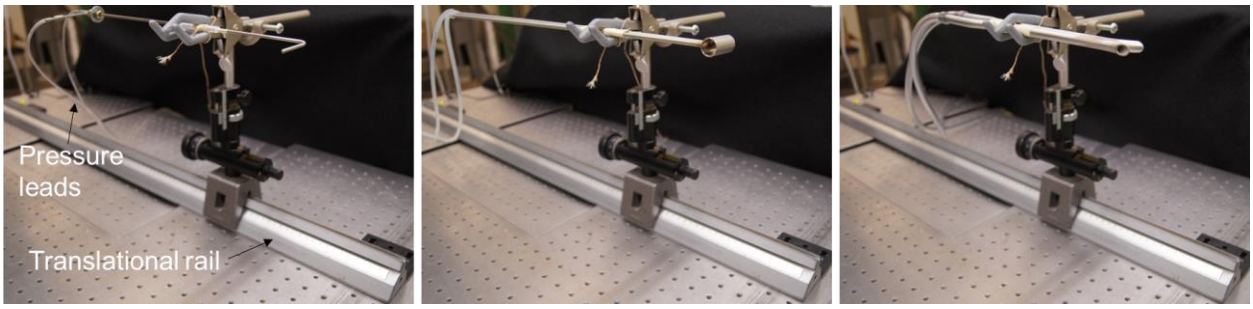

Fig. 8: The three probe types shown mounted on the translational rail for flow measurements in the wind jet.

2.3. Instrumentation and Data Acquisition

The operating principle of the three probe types is similar. Each probe measures the total and static pressure. The pressure differential between the two ports, ΔP, is measured utilizing a capacitance manometer (MKS 220CD Baratron). During the wind tunnel tests, the monitoring pitot probe was connected to a second capacitance manometer (MKS 220DD Baratron). Both manometers were calibrated against the National Fire Research Lab's (NFRL) working standard for pressure (NFRL WSTD 577967). Data from the manometers was acquired using a networked data acquisition board (NI cDAQ-9188) containing inputs for voltage and temperature. The data was then recorded using NFRL's custom data acquisition program, MIDAS. The velocity is then calculated within MIDAS, from the Bernoulli equation such that:

$$V = C_{pb}\sqrt{\frac{2\Delta P}{\rho}} \tag{1}$$

The air density, ρ, was calculated using the temperature (T) measured at the probe using a thermocouple (Omega Type K) and the ambient air static pressure, P_s:

$$\rho = \frac{P_s M}{RT} \tag{2}$$

Where M is the molecular mass of air and R the ideal gas constant. C_{pb} represents the probe coefficient for each respective probe.

3. Results

3.1. Probe Comparison – Wind Tunnel

Characterization of the wind tunnel flow with respect to fan set point was verified using two pitot probes. Measurements from the probes were acquired simultaneously. Fig. 9 shows the flow response to be linear over the range of fan settings. For flows greater than 2 m/s, the flow is steady with less than 1 % variation. The discrepancy between pitot probe measurements is less than 0.3 % on average, confirming the flow response at the test section.

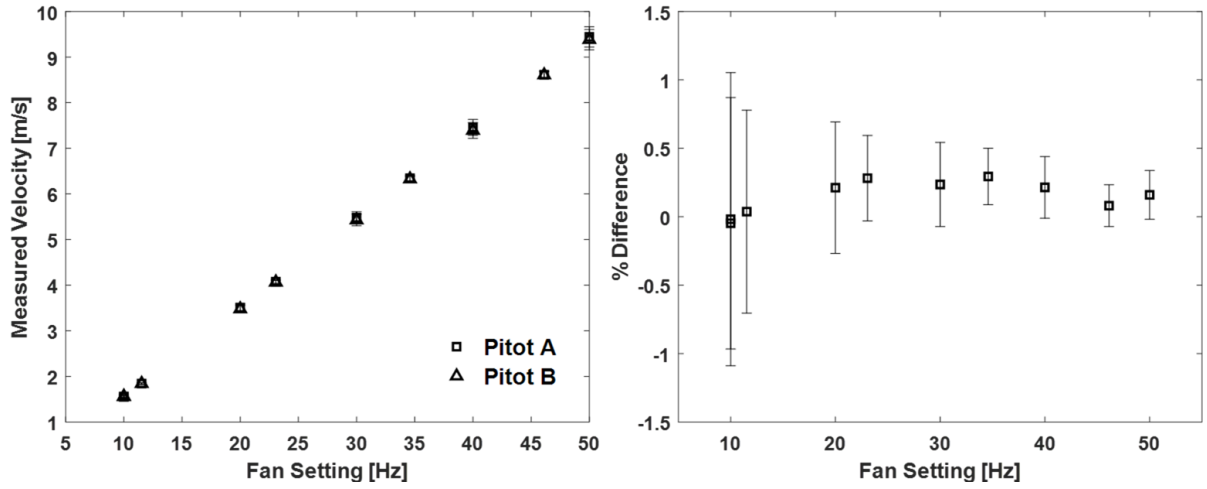

Fig. 9: Test section flow verification utilizing two different pitot probes. On the left is the wind tunnel flow response and the right shows the percent difference between the pitot probe measurements Error bars represent the estimated expanded uncertianty of the mean velocity measurement.

The results from all the probes tested in this study are summarized in Fig. 10. The *x*-axis indicates the response from a pitot probe taking simultaneous measurements, and the *y*-axis corresponds to the measured velocity from the probe under consideration. The velocity (Eq. 1) was calculated with a probe coefficient, C_{pb} = 0.93, for the bi-directional probes and C_{pb} = 0.83 for the S-probes. Overall, both the S-probes and bi-directional probes perform similarly, matching the velocity measured by the pitot probe (C_{pb} = 1).

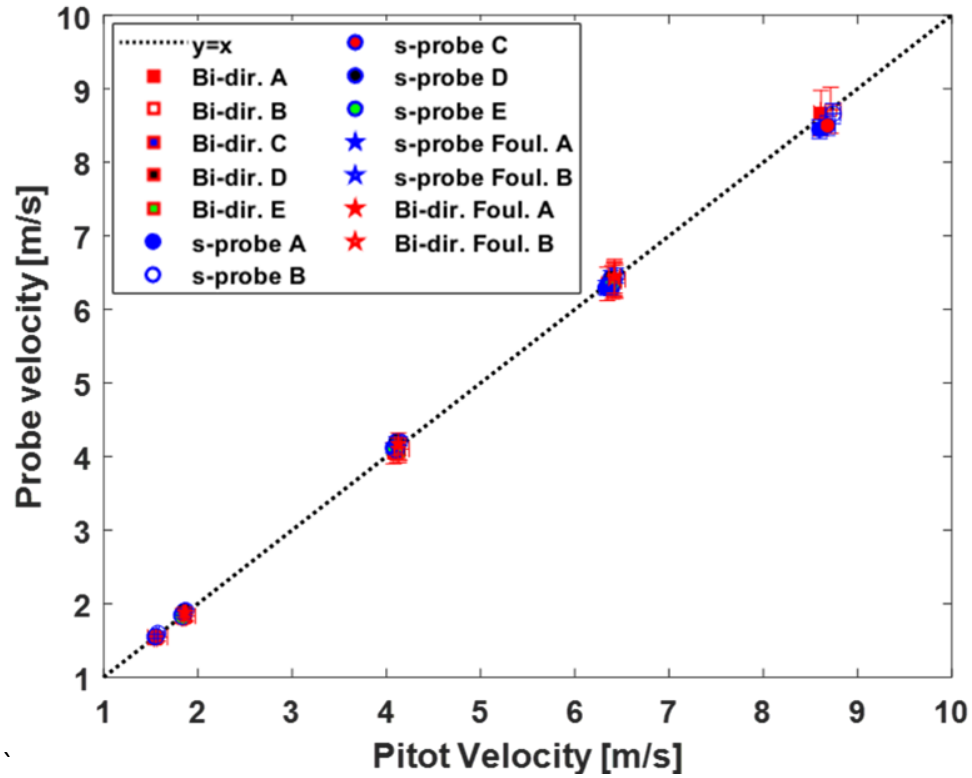

Fig. 10: The measured probe velocity compared to the pitot velocity. The y=x is the line of parity between the two measurements. Error bars represent the estimated expanded uncertianty of the mean velocity measurement.

Broadly speaking, the probes performed similarly, however in order to examine the accuracy of each probe, the percent difference from the pitot probe measurement was calculated, as shown in Fig. 11. Both types of probes become more accurate as the velocity increases. At the lower flow speeds, the maximum observed difference was approximately 2.5 % for S-probes and -3.0 % for the bi-directional probes; the negative sign indicating that the bi-directional probe was underpredicting the pitot probe. For flow less than 7 m/s, the S-probes tended to over predict while the bi-directional probes underpredicted. The opposite trend was observed at higher flows. Most measurements, however, fell within ±1 % for both types of probes. The fouled probes did not show any diminished accuracy compared to new or unused probes.

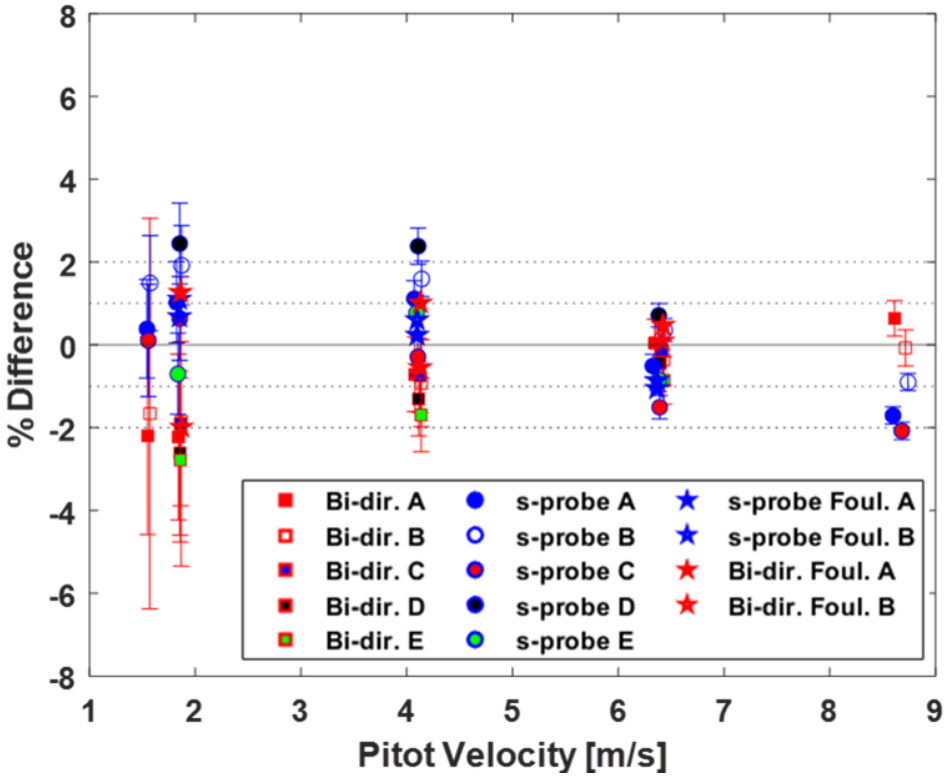

Fig. 11: Percent difference from the measured pitot probe velocity by each respective probe. Error bars represent the estimated expanded uncertianty of the mean velocity measurement.

The standard deviations from the respective probes are shown in Fig. 12. The well-conditioned flow results in measurement fluctuations less than 2 %. However, the impact of probe type or geometry is still apparent. Measurements from the pitot probe show a standard deviation consistently below 1% of the mean and decreasing to approximately 0.5 % at higher flow speeds. The S-probe and the bi-directional probe both demonstrate standard deviations larger than the pitot probe measurements. Generally, the standard deviation of flow measurements is linked to fluctuations in the flow. In wind tunnels, unsteady flow is common at low fan speeds [20, 21]. This is demonstrated in Fig. 12, as the standard deviation decreases for all probes as the fan (flow) speed increases. Despite the low level of fluctuations, the impact of probe geometry is consistent across the range of flow speeds, showing measurements from the bi-directional probe with the largest standard deviation, followed by measurements from the S-probe and then the pitot probe. The larger cross-sectional area of the bi-directional and S-probes lead to a larger wake region on the leeward side. Vortex shedding occurs in the wake region generating larger pressure fluctuations at the bi-directional and S-probes as shown in Fig. 12.

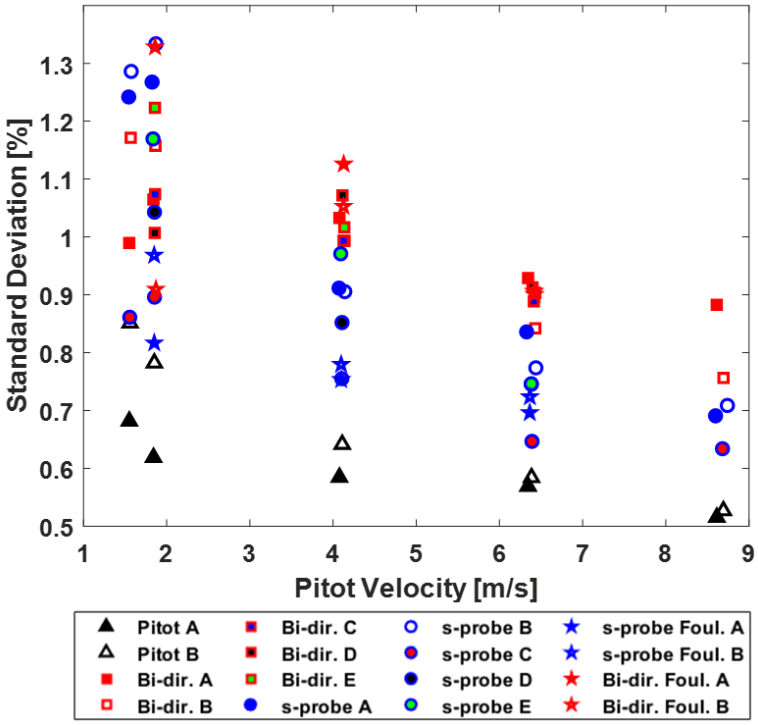

Fig. 12: Standard deviation of the wind tunnel flow speed measurements

In the characterization of bi-directional probes, McCaffrey and Heskestad [5] proposed a polynomial equation to determine the flow coefficient for bi-directional probes based on the Reynolds number (*Re*) of the flow. The flow coefficient was needed to correct the differential pressure measurements to match the velocity measurements from pitot probes or hot-wire anemometers. Because the equation was based on an empirical fit, it is only applicable for *Re* between 40 and 3800. If the expected *Re* was large or expected to fluctuate, they go on to state that using a constant flow coefficient of 0.93 would result in a maximum error of about 7 %. Characterizations of S-probes found flow coefficients ranging from 0.83 to 0.84 [18, 22].

Using the pitot probe as the reference flow measurement, V_{ref}, calibrations for the S-probes and bi-directional probes were determined from the wind tunnel data. The calibration coefficients were computed by rearranging Eq. 1 to:

$$V_{ref} = \sqrt{\frac{2\Delta P_{ref}}{\rho}} = C_{pb}\sqrt{\frac{2\Delta P_i}{\rho}},$$

$$C_{pb} = \sqrt{\frac{\Delta P_{ref}}{\Delta P_i}} \tag{3}$$

Such that the square root of the ratio of measurements of ΔP gives the respective probe coefficient. Calibration coefficients for each probe are plotted in Fig. 12 for *Re* ranging from 800 to 8000. Accepted values of the probe coefficients and their associated uncertainty are also plotted for the S-probes (0.840 ± 0.025) and bi-directional probes (0.926 ± 0.065) [5, 9]. The

calibration coefficients determined in this study agree with the accepted values within their uncertainty limits. This is confirmation that properly fabricated S-probes and bi-directional probes should perform as expected when used within their limitations.

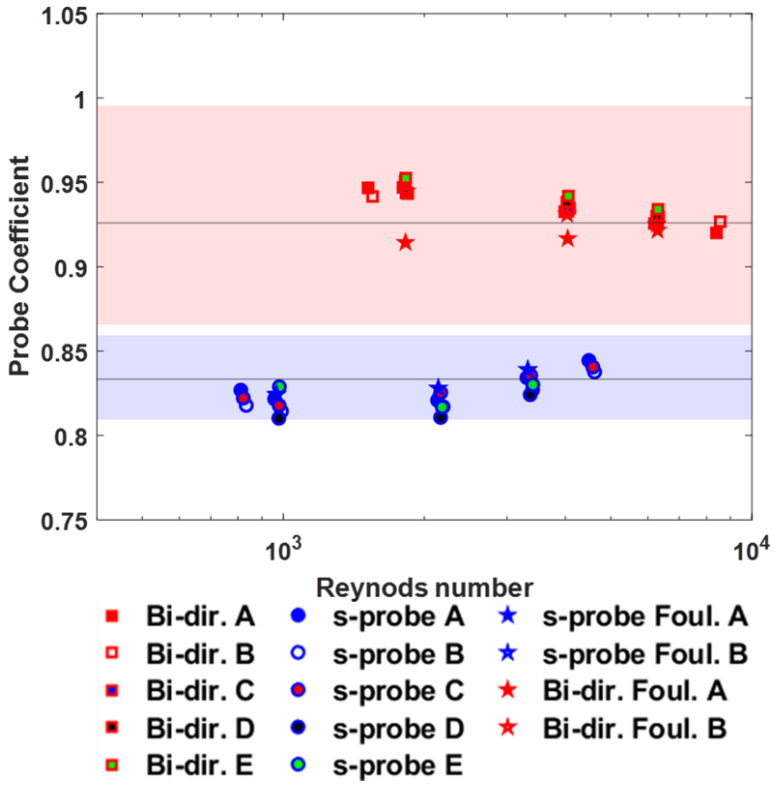

Fig. 13: Probe coefficient plotted against Reynolds number. The horizontal lines represent accepted values for the bi-directional probes and S-probes. The shaded regions correspond to the uncertainty of the accepted values.

3.2. Probe Comparison – Wind Jet

A wind jet was used to compare the probes under the realistic flow conditions of intermittency and turbulence present in fire-induced flows. The jet was generated using a centrifugal fan mounted to a table and the probes were used to measure the profile of the downstream flow. A diagram of a canonical flow from a turbulent jet [23] is shown in Fig. 14. The diagram demonstrates how the interface of the jet and the still ambient air forms a shear layer – the source of momentum decay, flow intermittency, and flow turbulence, that is characteristic of realistic flows. The velocity probes were placed sufficiently downstream such that a parabolic profile was expected, and the maximum velocity was lower than 10 m/s.

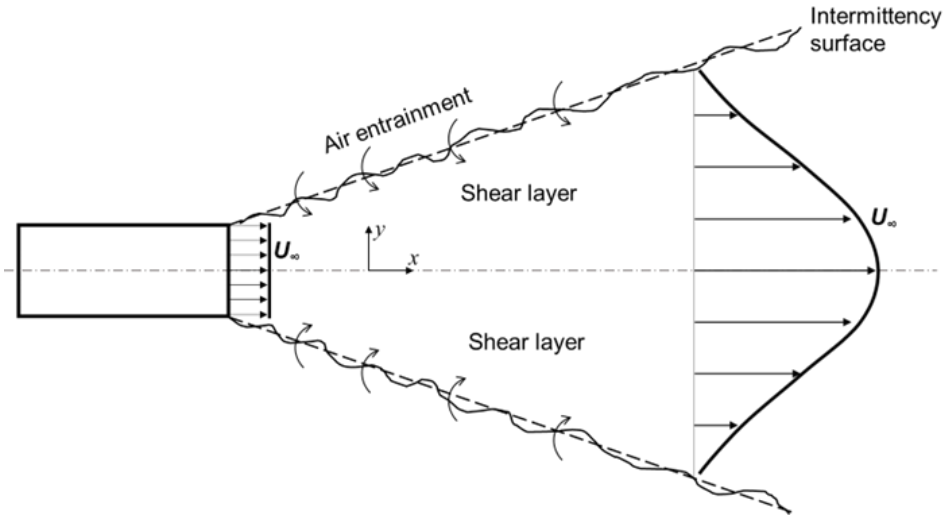

Fig. 14: Diagram of a typical jet flow and its downstream flow profile. The boundary between the jet and the ambient air creates a shear layer that leads to increased turbulence.

The velocity probes were traversed along a translation rail to measure the flow profile of the wind jet. Flow measurements are shown in Fig. 15., where markers represent the average of 3 traverses across the flow field. Traverses were conducted in 1 cm increments utilizing the 'A' probes and 2 cm increments utilizing the 'B' probes. In general, the flow field features a parabolic shape, typical of an unconfined jet. A 'core region' is estimated to exist between 15 to 31 cm as indicated by the approximately constant minima in the standard deviation across the profile (Fig. 16). A least squares regression was applied to fit a quadratic model to the average data points that follows the parabolic flow profile. All the regressions attained a R^2 value of 0.98 or higher. The regressions serve as a basis for comparison and not to predict or model the jet flow.

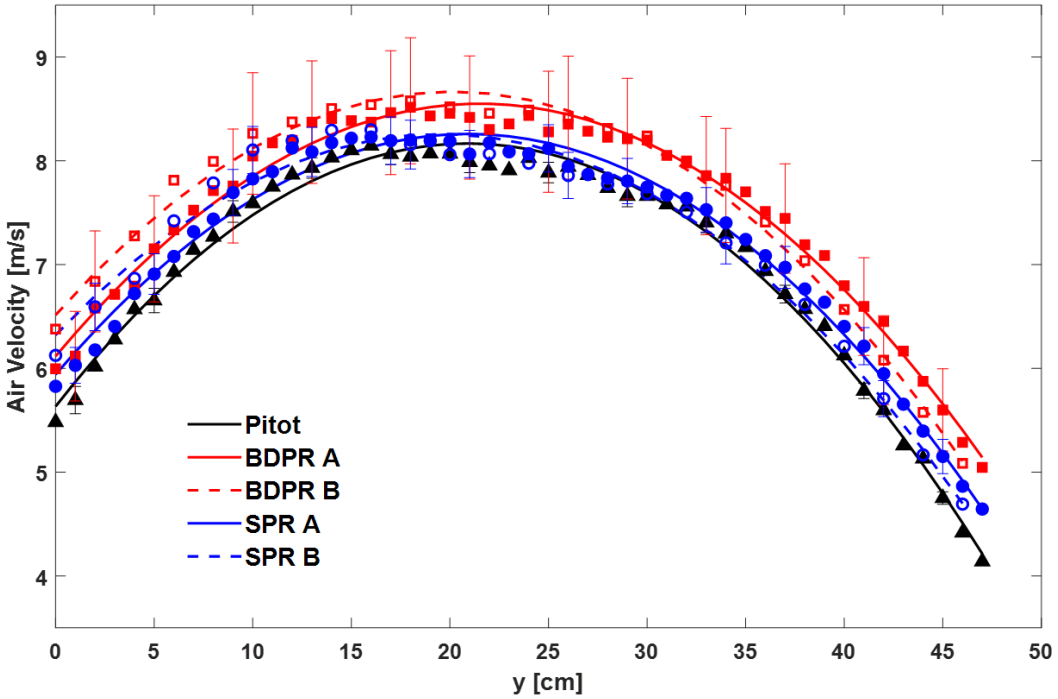

Fig. 15: Flow measurements from the wind jet. The markers are the mean velocity and the lines represent the regressions. Error bars represent the estimated expanded uncertianty of the mean velocity measurement.

The general comparison of the regression curves show that the pitot probe responded with the lowest flow speed while the bi-directional probe responded with the highest flow speed. The S-probe and pitot probe measurements show good agreement in the core region. In this region of the flow, it is easier to place the probes such that the flow is aligned perpendicular to the face of the probes. In the outer region or shear layer, the flow is more dynamic with greater flow intermittency and flow directionality. Therefore, the probes may not always be oriented for the best performance, especially the pitot probe which is sensitive to flow orientation. Both the S-probe and bi-directional probe demonstrate a larger deviation from the pitot probe measurements in the outer regions when compared to the core region. Since little effort was applied to align the probes with the flow for best performance, it is difficult to determine which probe gives the most accurate response when placed in the shear layer. Therefore, the shear layer comparison provides information on the potential range of responses from each of the probes.

The standard deviation (SD) and standard error of the mean (SEM) for the blower measurements are shown in Fig. 16. The fluctuations are consistent across all 3 probe types. As the probe is moved into the core region the standard deviation decreases as the flow speed encountered increases and the flow is hitting the probe face head on.

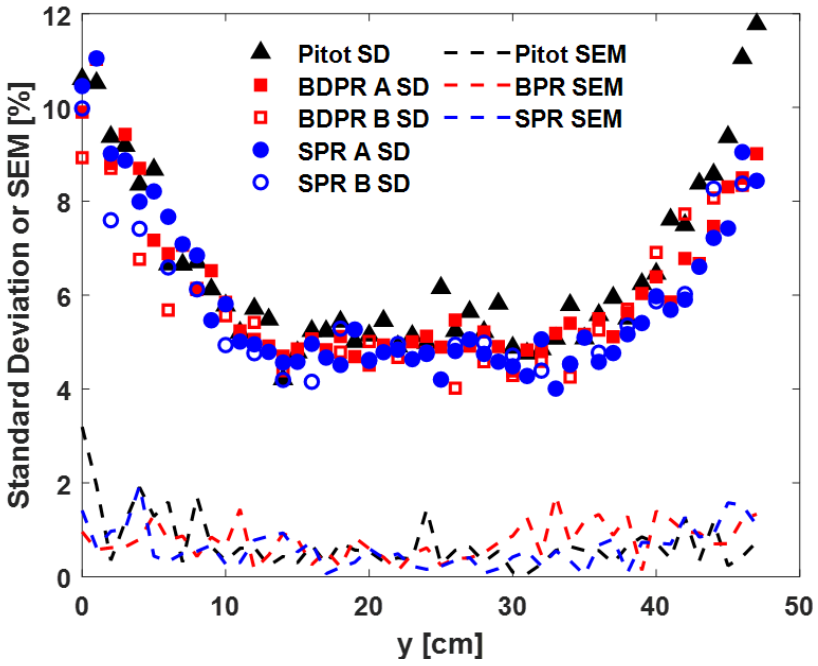

Fig. 16: Standard deviation and standard error of flow speed measurements from the wind jet.

Due to the turbulence, intermittency, and directionality of the flow each probe type responded differently. The probes were simply placed in the flow without being optimized to deliver their most accurate response. For this case, therefore, it is not prudent to establish one probe type as providing a more accurate measurement. Because the pitot probe consistently responded with the lowest flow speed, it is selected as an arbitrary reference measurement. Percent differences relative to the pitot probe measurement are plotted in Fig. 18. The differences were computed from the regression curves and demonstrate the range of responses from the different probe types. The regressions provide greater clarity to visualize the characteristics of the flow profile and allow for general comparisons of the large collection of measurements. In the core region, identified by the vertical lines, the differences in flow speed ranged from 0.2% to approximately 6.7 %, with the bi-directional probe providing the highest flow speed. At the shear region, the differences range from approximately 0.2 % to 22 %. In general, there is better agreement between the responses of the S-probe and pitot probe. Their agreement in the core region is consistent with the wind tunnel results (Fig. 11) and within the uncertainty limits for the S-probe.

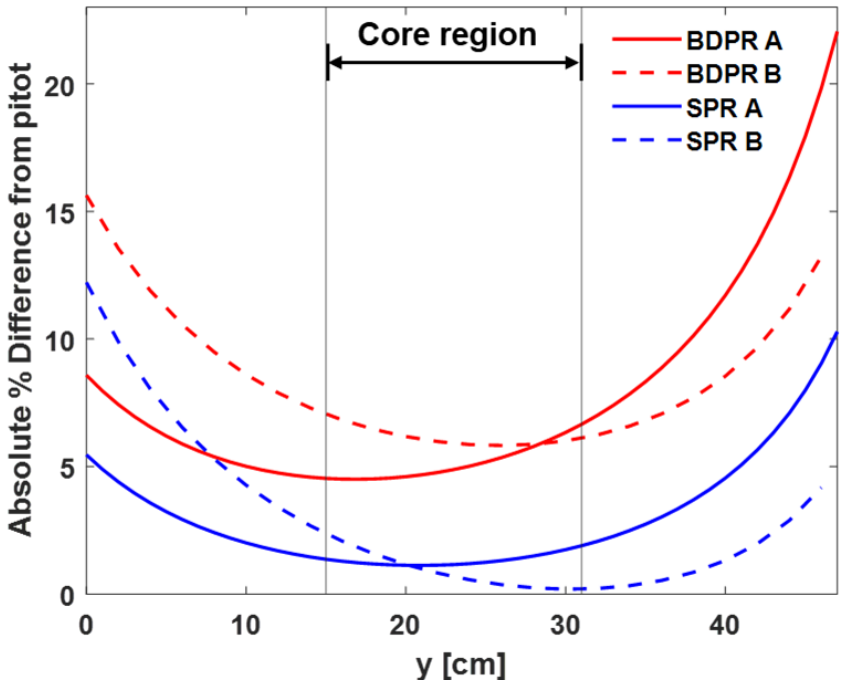

Fig. 17: Percent difference from the measured pitot probe velocity by each respective probe calculated using the respective data regressions.

4. Summary

This study documents the first published comparison of the performance of the S-type probe and the bi-directional probe - the most commonly used flow measurement device in fire research and testing. A traditional pitot static probe provided a reference for the comparison. When measuring well-conditioned, uniform flows from a research grade wind tunnel, the S-probe and bi-directional probe performed similarly. Probe calibration coefficients for both the S-probe and bi-directional probe were determined using the wind tunnel data and were in good agreement with accepted calibration coefficients from the literature and standard test methods. The agreement was observed across multiple probes from different manufacturing lots, with a subset having been exposed to high temperature and sooty conditions. Thus, properly fabricated and maintained probes should perform as expected when used within their limitations.

A comparison of flow speed measurements in the core region of a wind jet demonstrated good performance for both the S-probe and bi-directional probe. The differences were less than 7 % and within the uncertainty limits for each probe, with the bi-directional probe responding with the highest measurement of flow speed. Differences as high as 22 % were observed in the shear region, demonstrating the potential range of responses from the three probes when applied in a flow with characteristics of a fire-induced flow. It is possible that careful alignment of the probes within the shear layer flow would have resulted in better agreement.

Bi-directional probes are ubiquitous when measuring fire-induced flows. However, they are not readily available from commercial suppliers and the evidence to support their accuracy is

limited and dated. The S-type probe is the primary device for auditing flow measurements for smokestack emissions and thus has proven its capabilities in sooty and particle-laden flows. Numerous investigations have evaluated the accuracy of S-probes with respect to changes in shape, flow speed, and angular deviations, hence providing a greater knowledge base for the device. Most important the S-probe is available from a variety of commercial suppliers, some capable of providing calibration certificates for each device. For the first time the S-probe has been characterized with a side-by-side comparison to the bi-directional probe. Due to the similarities in design and operating principle, S-probes share many of the limitations of bi-directional probes, however, the results of this study demonstrate the S-probe performing as good or better than the bi-directional probe. Therefore, the S-probe is a suitable alternative to the bi-directional probe for measurements of fire-induced flow.

References

[1] Bryant RA (2011) Evaluating practical measurements of fire-induced vent flows with stereoscopic PIV. *Proceedings of the Combustion Institute* 33(2):2481–2487. https://doi.org/10.1016/j.proci.2010.06.105

[2] Dickinson MB, Wold CE, Butler BW, Kremens RL, Jimenez D, Sopko P, O'Brien JJ (2021) The Wildland Fire Heat Budget—Using Bi-Directional Probes to Measure Sensible Heat Flux and Energy in Surface Fires. *Sensors* 21(6):2135. https://doi.org/10.3390/s21062135

[3] Xu H, Pope I, Gupta V, Cadena J, Carrascal J, Lange D, McLaggan MS, Mendez J, Osorio A, Solarte A, Soriguer D, Torero JL, Wiesner F, Zaben A, Hidalgo JP (2022) Large-scale compartment fires to develop a self-extinction design framework for mass timber—Part 1: Literature review and methodology. *Fire Safety Journal* 128:103523. https://doi.org/10.1016/j.firesaf.2022.103523

[4] Bryant RA (2009) A comparison of gas velocity measurements in a full-scale enclosure fire. *Fire Safety Journal* 44(5):793–800. https://doi.org/10.1016/j.firesaf.2009.03.010

[5] McCaffrey BJ, Heskestad G (1976) A robust bidirectional low-velocity probe for flame and fire application. *Combustion and Flame* 26:125–127. https://doi.org/10.1016/0010-2180(76)90062-6

[6] Kent LA, Schneider ME (1987) The design and application of bi-directional velocity probes for measurements in large pool fires. 11–30.

[7] Method 2—Determination of Stack Gas Velocity and Volumetric Flow Rate (Type S Pitot Tube) (2000) (United States Environmental Protection Agency, Washington, DC USA). Available at https://www.epa.gov/sites/default/files/2017-08/documents/method_2.pdf

[8] D22 Committee Practice for Calibration of Type S Pitot Tubes. (ASTM International). https://doi.org/10.1520/D3796-09

[9] Stack Sampling Technical Information. A Collection of Monographs and Papers Vols. 1-4 (United States Environmental Protection Agency), EPA-450/2-78-042.

[10] Stationary Source Emissions - Measurement of Velocity and Volume Flowrate of Gas Streams in Ducts (International Organization for Standardization).

[11] Kang W, Trang ND, Lee SH, Choi HM, Shim JS, Jang HS, Choi YM (2015) Experimental and numerical investigations of the factors affecting the S-type Pitot tube coefficients. *Flow Measurement and Instrumentation* 44:11–18. https://doi.org/10.1016/j.flowmeasinst.2014.11.006

[12] Nguyen DT, Choi YM, Lee SH, Kang W (2019) The impact of geometric parameters of a S-type Pitot tube on the flow velocity measurements for greenhouse gas emission

monitoring. *Flow Measurement and Instrumentation* 67:10–22. https://doi.org/10.1016/j.flowmeasinst.2019.03.002

[13] Singh A, Khan IA, Khan MZ, Mahto P (2021) The effect of low Reynolds number on coefficient of S-type pitot tube with the variation in port to port distance. *Materials Today: Proceedings* 45:7810–7815. https://doi.org/10.1016/j.matpr.2020.12.174

[14] Li H, Zhang L, Yao X, Zhang J (2019) The application of numerical calculation method in determining the coefficient of S-type Pitot tube. *Journal of Physics: Conference Series* 1300(1):012117. https://doi.org/10.1088/1742-6596/1300/1/012117

[15] Zhou K, Liu N, Lozano JS, Shan Y, Yao B, Satoh K (2013) Effect of flow circulation on combustion dynamics of fire whirl. *Proceedings of the Combustion Institute* 34(2):2617–2624. https://doi.org/10.1016/j.proci.2012.06.053

[16] Lei J, Liu N, Zhang L, Satoh K (2015) Temperature, velocity and air entrainment of fire whirl plume: A comprehensive experimental investigation. *Combustion and Flame* 162(3):745–758. https://doi.org/10.1016/j.combustflame.2014.08.017

[17] Pinto C, André J, Viegas DX (2020) Double S-type Pitot Tube for velocity field study of fire whirls. *Flow Measurement and Instrumentation* 76:101806. https://doi.org/10.1016/j.flowmeasinst.2020.101806

[18] Bryant R (2023) An Automated System for Flow Characterization at Exhaust Ducts and Smokestacks. (National Institute of Standards and Technology, Gaithersburg, MD), NIST TN 2247, p NIST TN 2247. https://doi.org/10.6028/NIST.TN.2247

[19] Ramesh S (2023) Fire Resilience of a Steel-Concrete Composite Floor System: Full Scale Experimental Evaluation for Influence of Slab Reinforcement and Unprotected Secondary Beam (Test #3). (National Institute of Standards and Technology, Gaithersburg, MD), NIST TN 2267, p NIST TN 2267. https://doi.org/10.6028/NIST.TN.2267

[20] Mehta, RD, Bradshaw P (1979) Design rules for small low speed wind tunnels. *The Aeronautical Journal* 83(827):443–453. https://doi.org/10.1017/S0001924000031985

[21] Barlow JB, Rae WH, Pope A, Pope A (1999) *Low-speed wind tunnel testing* (Wiley, New York), 3rd ed.

[22] Kang W, Trang ND, Lee S, Lee SH, Choi YM (2020) Uncertainty analysis of stack gas flow measurements with an S-type Pitot tube for estimating greenhouse gas emissions using a continuous emission monitoring system. *Metrologia* 57(6):065031. https://doi.org/10.1088/1681-7575/ab9a9f

[23] Ball CG, Fellouah H, Pollard A (2012) The flow field in turbulent round free jets. *Progress in Aerospace Sciences* 50:1–26. https://doi.org/10.1016/j.paerosci.2011.10.002

Appendix A. List of Symbols

C_{pb}
calibration constant for probes

M
molecular mass

P_s
static pressure

ΔP
differential pressure

T
temperature

u
standard uncertainty

U
expanded uncertainty (95 % confidence interval, k = 2.0)

V
gas velocity

Greek

ρ
gas density

σ
standard deviation (repeatability)

Appendix B. Uncertainty Budgets

Estimates of measurement uncertainty were evaluated using the approximate methods described in the ISO GUM. [12] Measurement processes that were based on input measurements, x_i, were modeled as an output quantity, y:

$$y = y(x_1, x_2, x_3, \ldots, x_N) \quad \text{(B1)}$$

In the case that all input quantities, x_i, are uncorrelated, the relative combined standard uncertainty is given by

$$\frac{u(y)}{y} = \sqrt{\sum_{i=1}^{N} \left(s_i \frac{u(x_i)}{x_i} \right)^2} \quad \text{(B2)}$$

Where $u(x_i)$ is the standard uncertainty for each input, and s_i is the associated dimensionless sensitivity coefficient given by

$$s_i = \frac{\partial y}{\partial x_i} \frac{x_i}{y} \quad \text{(B3)}$$

Equation (B2) provides the propagation of uncertainty from each instrument and input parameter into the measurement model, Eq. (B1). The relative expanded uncertainty is defined as:

$$\frac{U(y)}{y} = k \frac{u(y)}{y} \quad \text{(B4)}$$

Where k = 2.0, is the coverage factor for the 95 % confidence interval.

Table 2: Uncertainty budget from the wind tunnel experiments at 4m/s showing the results from the three probes tested. The relative standard uncertainty is shown.

	Pitot		BD		SP	
x_i	Value	$u(x_i)/x_i$	Value	$u(x_i)/x_i$	Value	$u(x_i)/x_i$
C_{pb}	1	0.0050	0.9259	0.0350	0.83	0.0135
ΔP (Pa)	9.92	0.0090	11.39	0.0090	14.70	0.0090
R (J/kg•mol•K)	8314	0.0000	8314	0.0000	8314	0.0000
T (K)	295.7	0.0021	296.2	0.0021	295.4	0.0021
P_s *(Pa)*	101325	0.0100	101325	0.0100	101325	0.0100
M (g/mol)	28.97	0.0100	28.97	0.0100	28.97	0.0100
SEM	0.0009	0.0002	0.0010	0.0002	0.0016	0.0004
V (m/s)	4.08	0.0098	4.05	0.0360	4.12	0.0159

Table 3: Uncertainty budget from the wind jet experiments at y = 15cm showing the results from the three probes tested. The relative standard uncertainty is shown.

	Pitot		BD		SP	
x_i	Value	$u(x_i)/x_i$	Value	$u(x_i)/x_i$	Value	$u(x_i)/x_i$
C_{pb}	1	0.0050	0.9259	0.0350	0.83	0.0135
ΔP (Pa)	38.90	0.0090	48.60	0.0090	57.96	0.0090
R (J/kg•mol•K)	8314	0.0000	8314	0.0000	8314	0.0000
T (K)	297.9	0.0021	297.9	0.0021	298.5	0.0021
P_s *(Pa)*	101325	0.0100	101325	0.0100	101325	0.0100
M (g/mol)	28.97	0.0100	28.97	0.0100	28.97	0.0100
SEM	0.0009	0.0030	0.0010	0.0080	0.0016	0.0053
V (m/s)	8.10	0.0103	8.39	0.0369	8.22	0.0168